Numerical investigation of the effects of tunnelling on existing tunnels

V. Avgerinos
Geotechnical Consulting Group, London, UK; formerly Imperial College, London.
D. M. Potts
Department of Civil and Environmental Engineering, Imperial College, London, UK.
J. R. Standing
Department of Civil and Environmental Engineering, Imperial College, London, UK.

Abstract

Construction of the Crossrail tunnels just beneath the existing Central Line tunnels at the northern side of Hyde Park was the impetus for this paper. A basic 3D finite element (FE) model was developed to study a general case of a New Tunnel crossing perpendicularly below an Existing Tunnel. A series of 3D FE analyses was carried out and the results presented herein reveal some of the interaction effects. Changes in hoop forces, bending moments and lining deformations of the Existing Tunnel due to the New Tunnel excavation are discussed. Conclusions are drawn about how the relative position of the excavation face of the New Tunnel in relation to the Existing Tunnel axis affects the latter's behaviour. Cross-sectional and longitudinal deformations of the Existing Tunnel are discussed, leading to recommendations for field monitoring of similar interaction cases. Two parametric studies were also carried out to quantify the effects of: a) the magnitude of the EPBM face pressure; and b) the longitudinal stiffness of the Existing Tunnel on the predicted behaviour of the Existing Tunnel due to the New Tunnel construction.

Keywords

Tunnels, ground movements, numerical analysis, field monitoring

1 Introduction

As more tunnels are constructed in urban areas to facilitate infrastructure systems, the subsurface environment becomes more congested. The situation where a new tunnel is constructed in the vicinity of an existing tunnel is therefore becoming increasingly frequent. The consequent interaction has to be controlled: the existing tunnels need to remain operative during and after the completion of the new tunnel and consequently limits on allowable deformations should be specified (Kimmance et al., 1996).

Although field measurements of interaction between tunnels are generally rare, when available, they offer a valuable database for future design and an important reference against which numerical models can be validated (Cooper et al., 2002). The available field measurements of such problems generally identify three patterns of tunnel displacement and deformation: settlement, rotation and distortion. Table 1 summarizes tunnel-tunnel interactions, published from various case studies in London, in which field monitoring data were provided. In the case study of Cooper et al. (2002), the following observations were made based on the intensive monitoring performed.

a. The settlements of the existing Piccadilly Line increased with the successive construction of the three new Heathrow Express tunnels and in the long term, the asymmetry of the ground surface settlement troughs was attributed to the sequence of new tunnel construction.
b. The cross-section of the existing Piccadilly line tunnel, just above each of the new tunnels, rotated towards the excavation face as it approached and then, with further advancement of the face below and beyond it, it rotated in the opposite sense. The cross-section ultimately experienced a residual rotation which was asymmetrical around the new tunnels' alignments, a fact attributed to the relative skew angle between the new and existing tunnels.
c. The cross-section of the existing Piccadilly Line tunnel was distorted to an 'egg'-shaped form with its elongated axis following the face of the new tunnel excavation.

Numerical analysis has been used to obtain insight into the tunnel-tunnel interaction problem. The first tunnel-tunnel interaction problems that were investigated numerically considered tunnels with parallel axes. This general geometry can be investigated with plane-strain 2D analysis. Addenbrooke (1996) looked into different relative positions of tunnels with parallel axis in London Clay, focusing on the influence of spacing, rest period between their construction and construction sequence. For a side-by-side tunnel geometry, there is an interaction between the two tunnels when they are spaced less than 7 tunnel diameters apart. The first excavated tunnel 'squatted' due to the construction of the second, the second tunnel lining was generally stressed less than the first tunnel lining. An increased rest time masked the effect of the second tunnel on the first tunnel lining while the opposite was noted for the effect of the first tunnel on the second tunnel lining. For a piggy back

tunnel geometry, 4 tunnel diameters was found to be the critical vertical spacing between them. The influence of the second tunnel on the internal stresses of the first tunnel lining was more pronounced when the second tunnel was located below the first one with that influence being more pronounced with a decrease in the rest time (time between the two tunnels' construction).

Ng et al. (2004) investigated the interaction of two side-by-side tunnels, 20 m below the ground surface in London Clay, constructed with the New Austrian Tunnelling Method (NATM – now more commonly referred to as the Sprayed Concrete Lining method) using a 3D step-by-step approach (Katzenbach & Breth, 1981). The unsupported length (before constructing the lining) was 5m and the distance between the leading and the lagging tunnels was varied parametrically. The authors established the influence of the distance of the tunnels' faces on the surface settlement troughs. The authors also showed that the smaller this distance is, the more uniformly the loads were shared between the two tunnels. The larger this distance is the greater the bending moment that developed within the leading tunnel.

Liu et al. (2008) investigated for the Sydney region, the effects of tunnelling on an existing adjacent tunnel which was located 15 m below ground level with the new tunnel having horizontal, vertical or staggered parallel alignments. A step-by-step approach was adopted for the excavation of both tunnels with an unsupported length of 4 m. It was concluded that the shotcrete lining of the existing tunnel was significantly affected when the new tunnel face passed below it and was less affected as the new tunnel progressed further away from it. Their results indicated that the effect on the existing shotcrete tunnel lining differed for the various relative geometries considered.

As an extension, Liu et al. (2009) investigated the effect of perpendicularly crossing tunnels, also in the Sydney region, with a clearance of 3.5 m. They observed that the circumferential bending moments in the existing shotcrete lining was affected first in the leading side, then at the invert and the crown and finally at the far side as the new excavation progressed towards, under and beyond it. The interaction effect was restricted to a close area where the two tunnels crossed.

Clearly, not very extensive numerical research has been performed for the case where existing and New Tunnels do not have parallel axes. The impetus of this paper came from the Crossrail tunnels that were recently constructed beneath the existing Central Line tunnels in central London. The analyses were performed simulating the actual stratigraphy of the site and it was based on real Central and Crossrail tunnel dimensions and the clearance between them. However, since this paper investigates a more 'general' tunnel-interaction case, a single tunnel was modelled being constructed perpendicularly beneath an existing tunnel. The use of numerical analyses allows the

investigation of the interaction problem with regards to hoop forces, bending moment changes and deformation characteristics of the Existing Tunnel (ET) as the New Tunnel (NT) excavation is progressing. In all figures and subsequent sections the Existing and New Tunnels are referred to as ET and NT, respectively.

2 Description of the numerical model

2.1 General site information and stratigraphy adopted in the FE model

As already mentioned the impetus for this paper was the crossing of the new Crossrail tunnels beneath the existing Central Line tunnels, the former passing the latter at a 40° skew angle at the edge of Hyde Park. The Central Line tunnel axes are at 24 m below ground level and the Crossrail tunnels run below them with a relative crown to invert clearance that varies from 4.2 m to 4.9 m. The Crossrail tunnels were constructed using Earth Pressure Balance Machines (EPBM) within which conventional bolted precast concrete segmental lining rings were erected. Each ring is 1.5 m wide with internal and external diameters of D_{in}=6.2 m and D_{ex}=6.8 m respectively.

The adopted soil profile for the finite element analysis is presented schematically in Figure 1 and is based on the deepest of the boreholes sunk to install instrumentation at the greenfield site, HP6 (Wan et al., 2017). In the profile adopted there is a 6-m thick layer of superficial deposits (comprising made ground, alluvium and terrace gravels) overlying units B2, A3 and A2 of the London Clay (King, 1981) which have thicknesses of 30 m, 12.5 m and 11.4 m respectively. The London Clay is underlain by the Lambeth Group which has been divided into two layers representing the upper more clayey and less permeable units and the lower more granular and more permeable units.

2.2 Analyses performed and analysis sequence

Several analyses were performed, each one involving various stages spread over several increments. The excavation and construction of the Existing Tunnel was achieved using a volume loss control procedure (Potts and Zdravković, 2001). The target volume loss assumed for construction of the Existing Tunnel was V_L=1.6% (a reasonable estimate for open-face shield tunnelling in London Clay) with construction completed in less than 100 hours. It should be mentioned that for the original Central line tunnel each ring was erected in less than 20 minutes (Dalrymple-Hay & Jenkins, 1900). A 100-year period of consolidation followed. The New Tunnel length considered in the FE analyses was 120 m and the rate of excavation/construction modelled as 100m/week assuming an excavation length of 2 m (discussed further in Section 2.3.3).

In the primary analysis discussed in this paper, the New Tunnel was excavated assuming the face pressure of the EPBM to be 200 kPa (which was the mean face pressure measured by eight face pressure transducers inside the EPBM plenum chamber in the case of the westbound Crossrail tunnel in the vicinity of the intersection with the Central line tunnels). Volume losses are not an input in the 3D FE analyses presented herein. The volume loss obtained from numerically modelling construction of the New Tunnel is an output of the analyses and depends on the way that the modelling is performed (see Section 2.3.3). Generally 3D FE tunnelling analyses produce volume losses that exceed these measured in the field as a result of too large unsupported excavation length. However results of such analyses can be scaled to a desired volume loss as discussed by Franzius and Potts (2005).

Two series of parametric analyses were also performed in order to investigate:

a) varying the face pressure of the EPBM; and
b) varying the longitudinal axial and bending stiffness of the Existing Tunnel lining (using shell elements).

2.3 Analyses details

2.3.1 General

A 3D FE model was constructed in order to investigate in both an accurate and a computationally efficient way the tunnel-tunnel interaction problem. As far as the general geometry of the model is concerned, the following were considered:

i. One Existing Tunnel with diameter D_{ET} = 3.8 m and one New Tunnel with diameter D_{NT} = 6.8 m were simulated with their axes crossing perpendicularly to take advantage of symmetry.
ii. The clearance between the invert of the Existing Tunnel and the crown of the New Tunnel was assumed to be 5 m.
iii. Each ring of the New Tunnel was modelled to be 2.0 m in width. The 2 m excavation length (L_{exc}), is small enough not to result in an unrealistically high volume loss but is somewhat longer compared with typical concrete rings used in recent projects (e.g. Crossrail rings were 1.5 m wide).

The 3D finite element mesh used in the analyses is presented in Figure 2. It consists of 21528 20-noded hexahedral isoparametric solid elements, for modelling the soil, and 1031 8-noded shell elements (Schroeder, 2003) for modelling the two linings, 719 of which simulate the New Tunnel

lining. The axis of the Existing Tunnel runs along the x direction (from 0m to -110m) and the axis of the New Tunnel runs along the z direction (from 120m to 0m).

The FE mesh dimensions were selected carefully in view of their potential influence when analysing boundary value problems involving tunnelling, as highlighted by Franzius and Potts (2005). The New Tunnel length to be excavated was 120m (i.e. L_{tun}=120 m almost $20D_{NT}$) and the vertical boundary of the mesh perpendicular to its axis was placed at a distance of 50m (L_{soil}=50 m around $8D_{NT}$) in front of the final position of the face (see Figure 2). Both L_{tun} and L_{soil} were proven to be of sufficient length since 'steady-state' conditions were achieved for the final position of the New Tunnel face (described when the results are presented later). The Existing Tunnel was located halfway along the excavated length of the New Tunnel.

Each node of the solid elements has three degrees of freedom, one for each component of displacement (u, v and w) and the 8 corner nodes have an additional one for the pore water pressure degree of freedom. The shell elements have the same three displacement degrees of freedom and in addition three rotational degrees of freedom.

The analyses performed involved coupled consolidation for all solution increments. All the analyses were performed with the Imperial College FE Program (ICFEP) in 3D and 2*2*2 integration was used. An accelerated modified Newton-Raphson technique with an error-controlled substepping stress point algorithm was used as the solver for the non-linear Finite Element equations (Potts & Zdravković, 1999). Each analysis took between 15 and 20 days to run.

2.3.2 Modelling of soil and tunnel linings

A pre-yield non-linear elastic model (model J4, based on Jardine et al., 1986) coupled with Mohr-Coulomb yield and plastic potential surfaces was used for all the soil layers apart from the superficial deposits which were modelled as linear elastic perfectly plastic with Mohr-Coulomb yield and plastic potential surfaces. The pre-yield model (J4) has been described and calibrated by various researchers (e.g. Addenbrooke et al., 1997). The parameters for the non-linear elastic model J4 and for the Mohr-Coulomb model for all the soil layers are tabulated in Tables 2 and 3 respectively. During consolidation between the two tunnelling events, the angle of dilation, *v,* of the soil layers was set to zero to prevent the Mohr-Coulomb model from predicting unrealistic dilation in parts of the mesh where the soil yields. This assumption concerning the angle of dilation is believed not to affect the results since the soil's behaviour due to tunnelling is primarily affected by soil's stiffness and not strength.

Anisotropic permeability profiles, with permeability values reducing with depth, were assumed as shown in Figure 3a. These are consistent with the under-drained pore water pressure profile measured at the Hyde Park site close to the intersection of the Crossrail and Central line tunnels (see Figure 3b) and were used in the FE analysis. The K_0 profile used in the FE analysis is shown in Figure 3c.

The tunnel linings were represented by elastic isotropic shell elements (Schroeder, 2003). Each ring of the Existing Tunnel lining is formed of 26 elements while the half perimeter of the new lining is formed of 12 shell elements. The joints between segments and rings were not modelled. The Existing Tunnel lining was modelled assuming properties of grey cast iron, i.e. a unit weight of γ=69.16 kN/m^3, Young's modulus of E=100000 MPa and Poisson's ratio of μ=0.26 while the shell thickness was set as t=0.0781 m to match the second moment of area per unit metre of the original segment. The New Tunnel lining was modelled with γ=30 kN/m^3, E=40000 MPa, μ=0.15 and t=0.30 m, properties that simulate segments used for the Crossrail (bolted precast concrete segments grade of C50/60 concrete with steel fibre dosage of 30-kg/m^3). The shear correction factor for both tunnel linings was k=0.8. Finally, for the analysis where the longitudinal stiffness of the Existing Tunnel lining was reduced, as a means of simulating the joints between successive rings, anisotropic elastic shell elements were used to model the lining with their longitudinal axial and bending stiffnesses being 1% of the circumferential stiffness.

2.3.3 Boundary conditions

Throughout each analysis, movements in all the three directions (x, y and z) were restricted on the bottom boundary of the 3D mesh. All the lateral boundaries were prevented from moving in a direction normal to the boundary while the remaining components were not restricted. The top boundary of the mesh was free to move.

The Existing Tunnel excavation was modelled with the volume loss control method (Potts and Zdravković, 2001), implying plane-strain conditions. The excavation/construction of the New Tunnel followed a step-by-step approach (Katzenbach & Breth, 1981) modelling also the face pressure of the EPBM used (see Figure 4). In each increment of the excavation/construction of the New Tunnel, soil elements in front of the previous face position are excavated and simultaneously a pressure is applied to the New Tunnel face which is located at L_{exc} in front of the previous tunnel face. The shell elements representing the lining are also constructed during this increment but their stiffness is only activated at the end of the increment allowing soil movement into the tunnel. When the tunnel is advanced again, the next set of soil elements is excavated and consequently the active boundary of

the mesh changes and the face pressure which was applied on the previous boundary disappears with the excavated elements. This procedure was repeated for all of the tunnel excavation steps.

As the analyses employed coupled consolidation, it was necessary to define hydraulic boundary conditions. No change of pore water pressures was applied throughout the analyses either at the top of the London Clay or at the bottom of the Upper Lambeth Group, leaving their interface with the non-consolidating elements (of the superficial deposits and Lower Lambeth Group) free to drain (or take in water). During the excavation of the Existing Tunnel and the subsequent 100-year consolidation period the two lateral boundaries (normal to the z direction) were free to drain (i.e. no change in pore water pressure) being far away from the tunnel. The remaining two vertical boundaries (normal to the x direction) were impermeable as they are planes of symmetry for that stage of the analysis. During the New Tunnel excavation all the vertical boundaries were considered impermeable apart from the one which is far away from its axis (normal to the x direction) which was left free to drain. Around the perimeter of the Existing Tunnel a zero pore water pressure was prescribed allowing water to flow into the tunnel (simulating a permeable lining). No flow from the Existing Tunnel to the surrounding soil was encountered as its excavation procedure did not generate tensile pore water pressures in the surrounding soil. Finally, the completed New Tunnel was assumed to be fully impermeable. It should be noted that the pore water pressure profile prior to the New Tunnel excavation is not the same as the one assumed in the beginning of the analysis (see Figure 3a), it varies spatially, and depends on the permeability of the soil, the permeability assumed for the Existing Tunnel and the initial profile itself.

3 Surface soil movements due to the new excavation

In Figure 5, three monitoring areas are defined in the plane transverse to the existing (hence along the length of the New Tunnel). Throughout the paper these areas are consistently referred to as: behind; at; and in front of the Existing Tunnel axis.

As the New Tunnel progresses in the analysis, transverse surface settlements develop. These are presented in Figure 6a for the section located directly above the axis of the Existing Tunnel. A ‘steady-state’ is reached for the last 20 m of the New Tunnel advancement in front of the Existing Tunnel, where negligible additional settlements occur (less than half a millimetre), indicating that the results can be considered reliable and are not significantly influenced by boundary effects.

With regard to the shape of the surface settlement trough, the results from the analysis indicate that it does not change either for various positions of the New Tunnel excavation face in relation to a certain monitoring section or between different 'monitoring sections'. The normalised settlement troughs relating to the final New Tunnel face position (i.e. 120 m from the boundary of the mesh where tunnelling starts) as determined for different monitoring sections are presented in Figure 6b and are practically identical. This implies that in a transverse direction (to the New Tunnel axis) the presence of the Existing Tunnel does not affect the width/shape of the surface settlement troughs.

The evolution of volume loss with the advancing New Tunnel excavation face for a number of monitoring sections is presented in Figure 7. It can be observed that the rate of increase in volume loss diminishes considerably over the final 20 m of the New Tunnel advance for each of the monitoring sections apart from that at +30 m from the Existing Tunnel (where settlements are still developing). This further illustrates that a satisfactory 'steady-state' was reached for most of the mesh, especially in the close vicinity of the Existing Tunnel. Arrows are marked above each curve in Figure 7 to indicate the position at which the tunnel face reaches the corresponding monitoring section. The variation of volume loss along these points (illustrated with a thick grey dotted line) indicates that the rate at which the surface settlements develop is affected by the presence of the Existing Tunnel, despite the fact that the ultimate volume loss at the end of the New Tunnel excavation is constant for all monitoring sections. It seems that the earlier construction of the Existing Tunnel has caused the soil adjacent to it to soften, as evident from the larger volume losses behind the Existing Tunnel. The effect of softening the ground around the Existing Tunnel was offset to a degree in its close vicinity by the intrinsic stiffness of the tunnel itself (as evident from the small decrease in volume loss in the region close to its axis).

Longitudinal surface settlement profiles along a monitoring line located vertically above the New Tunnel axis for different New Tunnel excavation face positions (every 10 m) are shown in Figure 8. Arrows mark the position of the face for each curve. The profiles for the first 50 m of the New Tunnel excavation (grey lines), i.e. behind the Existing Tunnel, have the expected shape of a cumulative distribution curve (Attewell & Woodmann, 1982). As the New Tunnel excavation progresses, passing below and in front of the Existing Tunnel, the profiles distort from the form of a cumulative distribution and exhibit a localised maximum settlement behind the Existing Tunnel axis. The position of the maximum settlement moves towards the Existing Tunnel axis, reaching a maximum value of about 14.5 mm, 15-20 m behind it, where it becomes stable. As the New Tunnel excavation advances further, the surface settlements decrease locally around the Existing Tunnel because of the greater stiffness of the lining compared with that of the surrounding soil. Therefore, in the vicinity of

the New Tunnel, a combined effect of soil relaxation (due to the excavation/construction of the Existing Tunnel) and a stiffening of the ground (due to the presence of the Existing Tunnel) are revealed as the New Tunnel excavation progresses.

4 Existing Tunnel response

4.1 Hoop force and bending moment

Circumferential hoop force, bending moment distributions and the respective interaction diagram around the tunnel lining for various stages of the New Tunnel excavation are presented in Figure 9.

The distribution of hoop forces (Figure 9a) is almost uniform, fluctuating around an average of about -370 kN/m prior to the beginning of the New Tunnel excavation (n.b. the sign convention usually adopted in structural engineering is used where compressive forces are negative). It remains almost constant until the New Tunnel face reaches 10m behind the Existing Tunnel axis, at which point it starts becoming less uniform. The distribution reaches its most non-uniform state when the New Tunnel face is just below the axis of the Existing Tunnel. At this stage the hoop forces are up to 20% more compressive in the first and third quadrants and up to 30% less compressive in the second and the fourth quadrants (see inset diagram and defined zone in Figure 9a) compared with the situation prior to the beginning of the New Tunnel excavation. With further tunnel advance the hoop forces equilibrate to a new distribution and remain practically unchanged for the last 30 m of the New Tunnel excavation. At this stage the hoop forces are up to 10% more compressive around the crown and up to 10% more tensile everywhere else compared with the situation prior to the New Tunnel excavation.

The circumferential bending moments, which are practically zero prior the beginning of the New Tunnel excavation, follow a similar trend to that of the hoop forces (see Figure 9b). As the New Tunnel approaches the Existing Tunnel axis, the arcs of the sections of the lining in the first and third quadrants, defined by the horizontal axis of the tunnel and the position of its right shoulder and its left haunch, respectively, (looking in the negative x direction) start experiencing tension at the extrados. The remaining part of the lining experiences tension at the intrados. The change in the bending moments (relative to values prior to the new excavation) becomes a maximum (±12 kNm/m) when the new excavation face is below the axis of the Existing Tunnel. Generally an anticlockwise rotation of the lining sections experiencing tension at the extrados is evident with advancement of the New Tunnel. At the final stage of the New Tunnel-excavation the difference in the bending moments (compared with prior to its excavation) are ±4 kNm/m.

The combined effect of hoop force/bending moment acting on different positions of the ring (for any New Tunnel face position) are well within the failure envelope of the analysed section of the Existing Tunnel (see Figure 9c). This indicates that despite the sizeable changes in hoop force and bending moment, no structural failure (e.g. cracking of the lining) is predicted due to the New Tunnel excavation either in the temporary condition or after the New Tunnel construction has progressed far away from the intersection area.

4.2 Overall deformations

Overall deformed shapes of the Existing Tunnel as the New Tunnel excavation progresses are shown in Figure 10 along with superimposed contours of displacement (representing a combination of all three components).

The Existing Tunnel lining starts experiencing displacements and deformations due to the new excavation when the excavation face is about 40m behind its axis (Figure 10a). With further advancement of the New Tunnel the magnitude of both increases (Figures 10b to f). The closer a section of the Existing Tunnel is to the New Tunnel axis, the greater and more rapidly it deforms while there is negligible influence at distances greater than 30 m to 40 m from the New Tunnel. Once the New Tunnel face is at greater distances from the Existing Tunnel (about 40 m in front of it) its overall deformed shape does not change indicating that the influence zone is no longer affecting it (Figures 10g and h).

As far as the magnitudes of the displacements are concerned, the vertical component (in the y direction) is the greatest with a maximum magnitude of around 23 mm, while displacements in the two horizontal directions are an order of magnitude smaller (longitudinally up to around 2 mm and transversely up to around 7 mm).

Two major modes of deformations can be noted from Figure 10 and are discussed in the following sections:

a. the Existing Tunnel's cross-section deforms elliptically, forming either 'squatting' or 'egg-shaped' profiles, and rotates as the New Tunnel advances (Standing and Selman, (2001) observed this mode of deformation with field measurements); and
b. longitudinal bending of the lining caused by its vertical settlement.

In the initial few metres of the New Tunnel advancement (Figure 10a) a lengthening of the horizontal axis and shortening of the vertical axis of the Existing Tunnel occurs. Viewing along the Existing Tunnel (negative x-direction), there is a resulting 'squatting' form that rotates anticlockwise as the New Tunnel advances towards the Existing Tunnel axis, with lengthening along a chord connecting

the left haunch to the right shoulder of the ring directly above the New Tunnel and shortening in the orthogonal direction. As the New Tunnel advances further, in front of the Existing Tunnel, the major axis of the latter's elliptical section has rotated so that it is essentially vertical, thus becoming 'egg-shaped' (Figure 10e). In all cases, deformations of the Existing Tunnel cross-section diminish with distance from the New Tunnel.

4.2.1 Cross-sectional deformations

Figure 11 presents the cross-sectional deformation of sections directly above the New Tunnel axis, and at distances of 10m and 20m in the form of changes in span of several chords. In practice, changes in such chords might be measured using a tape extensometer from within the Existing Tunnel. The changes in chords/diameters obtained from the finite element analysis show that their length remains unaffected until the New Tunnel face is about 30 m behind the axis of the Existing Tunnel. From that tunnel face position onwards, the following observations can be made from the results of the numerical analysis.

a. Diameter BD increases in length as the New Tunnel approaches the Existing Tunnel, reaching a maximum when its face is directly below the axis of the existing. It subsequently decreases as the New Tunnel progresses.
b. The behaviour of diameter AC (orthogonal to diameter BD) follows an almost mirror image mode to that of BD.
c. The chord BC, which connects the two haunches of the lining, increases in length as the New Tunnel approaches the Existing Tunnel, reaching a maximum when it is 5 m behind it. The span then reduces, reaching a minimum when the excavation face is 5 m in front of the axis of the Existing Tunnel, and then increases again before becoming stable with further tunnel face advancement.
d. Changes in length of the other chords (AD, AB and CD) are negligible being less than 1mm for any New Tunnel position (and so are not plotted in Figure 11).

For tunnel advancement beyond about 40 m in front of the Existing Tunnel, there are negligible further changes in the length of the chords/diameters and the deformed shape of the section remains (see both Figure 11 and Figures 10g and h).

As expected, the largest span changes are observed in the section just above the New Tunnel axis (Figure 11a) and their magnitude decreases with increasing distance of the section from the New Tunnel (Figures 11b and c). Note different scales are used for the changes shown in Figures 11a, b and c.

Figure 11 clearly identifies that, rapid changes in span lengths of the Existing Tunnel occur when the excavation face of the New Tunnel is in the close vicinity of the Existing Tunnel. Most significant changes in span length occur over approximately 20m of the New Tunnel excavation advancement (from -15m to +5m). Given that modern TBMs (in soil conditions like London Clay) can readily achieve advancement rates greater than 15m/day, Figure 11 suggests that when transient distortions are of interest and need to be measured in tunnel-tunnel interaction problems, remote automated measurement systems should be used. Monitoring such distortions using manual field measurements during 'engineering hours' is likely to result in key responses being missed.

The results shown in Figure 11 can be compared with the field measurements taken when the first Crossrail tunnel was excavated beneath the Central Line tunnels at Hyde Park, presented by Yu (2014), and show an overall satisfactory agreement in terms of the magnitude and the manner of changes in the chord lengths despite the simplified basic scenario analysed here.

4.2.2 Longitudinal strains

Findings from the numerical analysis regarding the development of longitudinal strains along the exiting tunnel crown and invert due to the New Tunnel excavation are summarized in Figure 12a and b. The influence of the new excavation first becomes evident at both crown and invert level when the face of the new excavation is about 10m behind the intersection of the two alignments. The magnitude of strains develops appreciably as the New Tunnel face advances from 10m behind to 10m in front of the Existing Tunnel after which they remain essentially constant.

The form of the longitudinal strains that develop in the crown (Figure 12a) is the same as would be expected in the ground transverse to a New Tunnel in greenfield conditions, with maximum compression strains directly above the tunnel axis, reducing laterally, becoming zero at a certain offset (the points of inflection when considering tunnelling in the greenfield condition). Tensile strains develop beyond these offsets (c.f. again points of inflection), reaching a maximum before diminishing towards zero with further distance. In the analysis, the offset distance from the axis of the New Tunnel at which longitudinal strains in the Existing Tunnel change sense is about 20 m (Figure 12a). As the New Tunnel advances, the magnitudes of the compressive and tensile strains increase. Ultimately, after the strain evolution stabilises, the maximum compressive and tensile longitudinal strains in the crown of the Existing Tunnel are 240 με and 60 με, located directly above and 32 m from the New Tunnel axis respectively with the offset where strains switch from compression to extension being 17.1 m (2.6*D) from it.

The mode of strains along the invert (Figure 12b) is slightly more complex with final maximum compressive and tensile strains being 120 με and 85 με, respectively.

The FE predictions of the longitudinal strains along the crown and the invert of the Existing Tunnel could be used in practice when assessing tunnel-tunnel interaction problems provided that the results are scaled to the design value of volume loss. This methodology was proposed by Franzius and Potts (2005) for a case where they analysed the tunnelling-induced transverse deformation of a building.

5 Parametric considerations

5.1 Influence of the face pressure of the EPBM

It is generally thought that the instruments measuring the pressure in the plenum chamber of an EPBM, measure lower pressures than those applied to the soil in front of the cutter-head. In order to investigate this further in relation to its effect on the Existing Tunnel's response, additional analyses were run, in which the face pressure applied in the model was set to 0 kPa and 500 kPa (n.b. a value of 200 kPa has been used in the analyses described so far – see Figure 9 for the distributions of absolute values of hoop force and bending moment with this face pressure). Increasing the face pressure is thought to contribute in reducing the rate of development and the magnitude of the ground surface settlements. However, in numerical analysis, the unsupported length (L_{exc}) seems to be a much more influential factor. The grout pressure behind the rings is not modelled herein and as such only the effect of face pressure is discussed.

The hoop forces developed in the Existing Tunnel for the three New Tunnel excavation face pressures are presented in Figure 13a and b (comparisons are made between the case with no face pressure and those with either 200 kPa or 500 kPa pressure). Generally hoop forces are within 5% all around the lining for any position of the New Tunnel excavation face irrespective of the face pressure, with the exemption of when it is 10 m behind the crossing. This result indicates that the stabilised hoop force distributions are not greatly affected by the EPBM face pressure. However, when the face of the new excavation is 10 m behind the crossing, an increase in the face pressure results in generally more compressive hoop forces with a maximum increase of 8% and 18% for face pressures of 200 kPa and 500 kPa respectively.

Equally, the circumferential bending moments (see Figure 13c and d) are mostly affected by the excavation of the New Tunnel when its face is 10m behind the Existing Tunnel axis with a maximum

difference of 5 kNm/m being monitored. Comparing Figure 13 to Figure 9, it can be concluded from the numerical analyses that an increase of the face pressure of the EPBM is beneficial for the circumferential bending moments of the Existing Tunnel for any position of the EPBM face, because a reduction in their magnitude at any point around the cross-section is predicted.

The results presented above suggest that in cases where the combined hoop force/bending moment within an existing lining are likely to become adverse because of the construction of a New Tunnel beneath it, there are benefits to increasing the EPBM face pressure.

The effect of not applying and applying 500 kPa face pressure on the deformation of the various cross-sections of the Existing Tunnel lining is shown in Figure 14. The results are presented in the same way as in Figure 11 (where the face pressure was 200 kPa). An increase in face pressure results in a delayed response of the Existing Tunnel with noticeable changes in span not starting until the face was within about 20m of it (compared with 30m when the modelled face pressure was 200 kPa). This is the case for all the sections considered (Figure 14a, b and c) regardless of their distance from the New Tunnel axis. As the New Tunnel advances further in front of the Existing Tunnel, the increased face pressure seems to cause the spans to change length more rapidly. Consequently the final stable lengths are different, although these effects diminish with increasing distance of the cross-section from the New Tunnel axis.

5.2 Influence of the longitudinal stiffness of the Existing Tunnel

The Existing Tunnel lining models a sequence of successive rings of bolted grey cast iron segments. In all the analyses presented so far, a rigid connection between successive rings was inherently assumed. This implies that the tunnel is actually simulated as a long continuous tube within the ground. In practical terms this could be interpreted as a situation where the circumferential bolts, connecting two successive rings, are very tightly tightened. This is not always the case and successive rings can have their bolted connections loose with circumferential bolts not being tightened. As a way of modelling the effect of an extreme case (where successive segments are practically unbolted) numerically, anisotropic shell elements were used to simulate the Existing Tunnel with their longitudinal axial and rotational stiffness reduced to be 1% of their circumferential values for the case when the face pressure applied in the numerical model is 200 kPa.

The evolution of the longitudinal strains along the crown and the invert of the Existing Tunnel when successive rings are modelled to be practically unbolted are presented in Figure 15. The shapes of the predicted strains along the crown and invert are generally similar to those in which the Existing Tunnel was modelled as a continuous tube (Figure 12). In this ‘loose ring’ case the magnitudes of

longitudinal strains are about six to ten times larger. This difference in the magnitude of strains for the two cases shows that for the 'loose ring' larger axial displacements are anticipated and consequently the stresses in the longitudinal direction are likely to reduce.

6 Conclusions

The series of 3D FE analyses presented have investigated the interaction and influence of a New Tunnel crossing perpendicularly beneath an Existing one. The motivation for the analyses presented herein was the new Crossrail tunnels excavated beneath the existing Central Line tunnels in central London. The results provide insight into the interaction problem with regard to changes in hoop forces, bending moments, cross-sectional deformations and longitudinal strains of the Existing Tunnel. The effects of the EPBM's face pressure and the longitudinal stiffness of the Existing Tunnel were also explored.

The predicted ground surface movements show that the presence of the Existing Tunnel affects the rate at which settlements develop for transverse sections near to it. The ground surface settlements also reflect a combination of the soil disturbance from the previous construction of the Existing Tunnel and of the stiffening of the ground due to its presence.

Regarding the structural capacity of the Existing Tunnel, the most critical combination of circumferential hoop force and bending moment is identified as the point when the New Tunnel excavation face is directly below the Existing Tunnel axis.

For the geometry investigated, the Existing Tunnel experiences deformations when the New Tunnel approaches to within 20 m of its axis. These deformations develop with further advance of the face of the New Tunnel and stabilise once it has reached a distance of 20 m beyond the Existing Tunnel axis. Various cross-sections of the Existing Tunnel deform into an elliptical shape as the New Tunnel face advances. The major and minor axes of the ellipse rotate as the New Tunnel advances, with the major axis following the New Tunnel's excavation face. It has been shown that the most significant changes occur over a very short distance (when the New Tunnel is in the very close vicinity of the Existing Tunnel) suggesting that remote in-tunnel monitoring (rather than manual measurements made during engineering hours) would be necessary to observe the complete tunnel response. Longitudinally, the most significant strains are predicted along the crown of the Existing Tunnel.

Results presented in this paper are for a certain volume loss. However, the results can be scaled to an appropriate volume loss in order to be used for a particular scenario as discussed by Franzius and

Potts (2005).

The influence of the face pressure of the EPBM was also studied parametrically. An increased face pressure acts generally beneficially for the Existing Tunnel, reducing the combined effects of lining hoop force and bending moment. Changing the longitudinal stiffness of the Existing Tunnel can be used as a means of modelling unbolted lining rings.

Acknowledgements

The authors wish to acknowledge the Engineering and Physical Sciences Research Council (EPSRC, research grant: EP/G063486/1), Crossrail and Morgan Sindall who were major sponsors of the research project at Imperial College. London Underground Ltd is also acknowledged as it kindly gave access to the research team in the Central Line tunnel for field measurements to be taken. Many thanks are due to the Imperial College research team, in particular Professor John Burland, Dr. Yu Jessica and Dr Katerina Tsiampousi.

References

Addenbrooke, T.I. 1996. *Numerical analysis of tunnelling in stiff clay*. PhD thesis, Imperial College, University of London, London, UK.

Addenbrooke, T.I., Potts, D.M. and Puzrin, A.M. 1997. *The influence of pre-failure soil stiffness on the numerical analysis of tunnel construction.* Géotechnique, Vol.47, No. 3, pp.: 693-712.

Attewell, P.B., & Woodman, J.P. 1982. *Predicting the dynamics of ground settlement and its derivatives caused by tunnelling in soil.* Ground Engineering, Vol.15, No.7, pp.: 13–22 & 36.

Barakat, M.A. 1996. *Measurements of ground settlement and building deformations due to tunnelling.* PhD thesis, Imperial College, University of London, UK.

Cooper, M.L. 2001. *Tunnel induced ground movements and their effects on Existing Tunnels and tunnel linings*. PhD thesis, University of Birmingham, UK.

Cooper, M.L., Chapman, D.N., Rogers, C.D.F. and Chan, A.H.C. 2002. *Movements in the Piccadilly line tunnels due to Heathrow Express construction*. Géotechnique, Vol.52, No.4, pp.: 243-257.

Dalrymple-Hay, H.H. & Jenkins, B.M. 1900. The Waterloo and City Railway. Minutes of Proceedings ICE, Vol.139, pp.:25-55 .

Franzius, J.N. & Potts, D.M. 2005. *Influence of mesh geometry on three-dimentional finite-element analysis of tunnel excavation*. International Journal of Geomechanics. Vol.5, pp.: 256-266.

Jardine, R.J., Potts, D.M., Fourie, A.B., & Burland, J.B. 1986. *Studies of the influence of non-linear stress-strain characteristics in soil-structure interaction*. Géotechnique, Vol.36, No.3, pp.: 377–396.

Katzenbach, R., & Breth, H. 1981. *Nonlinear 3D analysis for NATM in Frankfurt Clay*. Proceedings of the 10th International Conference of Soil Mechanics and Foundations Engineering, Vol.1., Balkema, Rotterdam, pp.: 315–318.

Kimmance, I.P., Lawrence, S., Hassan, G., Purchase, N.I and Tollinger, G. 1996. *Observations of deformations excavations created in existing tunnels by adjacent and cross cutting excavations*. Proceedings of the International Symposium on Geotechnical Aspects of Underground Construction in Soft Ground, City University, Pub AA Balkerna, London, pp.: 707-712.

King, C. 1981. *The stratigraphy of London Basin and associated deposits*. Tertiary Research Special Paper, Vol.6, Backhuys, Rotterdam.

Liu, H.Y., Small, J.C., Carter J.P. 2008*. Full 3D modelling for effects of tunnelling on existing support systems in the Sydney region.* Tunnelling Underground Space Technology, 2008, Vol.23, pp.: 399–420.

Liu, H.Y., Small, J.C., Carter, J.P., and Williams, D.J. 2009. *Effects of tunnelling on existing support systems of perpendicularly crossing tunnels.* Computers and Geotechnics, Vol.36, pp.: 880-894.

Ng, C.W.W., Lee, K.M, Tang, D.K.W. 2004. *Three-dimensional numerical investigations of new Austrian tunnelling method (NATM) twin tunnel interactions.* Canadian Geotechnical Journal, Vol.41, pp.: 523-539.

Potts, D.M., & Zdravković, L. 1999. *Finite Element analysis in geotechnical engineering: theory*. Vol.1. Thomas Telford, London.

Potts, D.M., & Zdravković, L. 2001. *Finite Element analysis in geotechnical engineering: application*. Vol.2. Thomas Telford, London.

Schroeder, F.C. 2003. *The influence of bored piles on existing tunnels*. PhD thesis, Imperial College, University of London, London, UK.

Selman, R. 1998. Subsurface settlements induced by tunnelling in London Clay. *Proceedings European Young Geotechnical Engineer's Conference.* Tallinn, Esthonia, pp.: 1-8.

Standing, J.R. & Selman, R. 2001. *The response to tunnelling of existing tunnels at Waterloo and Westminster. Building Response to Tunnelling: Case Studies from Construction of Jubilee Line Extension*, London: Vol.2: Projects and Methods. CIRIA Special Publication 200. London, Thomas, Telford. pp.: 509-546.

Wan, M.S.P., Standing J.R., Potts D.M. and Burland J.B (2017) *Measured short-term ground surface response to EPBM tunnelling in London Clay*, Géotechnique, Vol. 67, No. 5, pp. 420-445. (DOI: http://dx.doi.org/10.1680/jgeot.16.P.099)

Yu, J.B.Y. 2014. *Assessing ground interaction effects and potential damage on Existing Tunnels before and after new excavation works*. PhD Thesis, Imperial College London.

Table 1: Case studies (with available field data) of tunnel-tunnel interactions

Researcher	Field monitoring	Existing tunnels	New tunnels	Location	Position of new tunnel
Barakat (1996)	Settlement, distortion	Piccadilly T4 station; cast iron	Heathrow express	Heathrow terminal 4	Not reported
Kimmance et al. (1996)	Deformations	Northern line station	Northern line station; grey cast iron	London bridge	parallel (clearance: 5.8m)
Kimmance et al. (1996)	Deformations, settlement	Northern line running	Jubilee line extension	London bridge	Below (clearance: 2m)
Selman (1998)	Settlement, rotation and distortion	Bakerloo and Northern line running	Jubilee line extension; SCL method	Waterloo	Not reported
Selman (1998)	Settlement, rotation and distortion	District and Circle line running	Jubilee line extension; SCL method	Westminster	Not reported
Standing & Selman (2001)	Settlement, cross-sectional and longitudinal distortions and twisting	Northern and Bakerloo line running, Shell Centre water cooling tunnel; bolted grey cast iron segments	Jubilee line extension; SCL method	Waterloo	below (clearance: 5.6m-9.8m)
Cooper (2001)	Settlement, rotation and distortion	Piccadilly line running	Heathrow express vent	Heathrow terminal 4	below (clearance: 5.4-12m, skew angle: 45º)
Cooper (2001)	Settlement, rotation and distortion	Mainline railway tunnels	Enlargement of Northern line running	Old street station	parallel (clearance: 5.0m)
Cooper et al. (2002)	Settlement, rotation and distortion	Piccadilly line running; unbolted concrete segments with specially designed longitudinal joints	Heathrow express - 3 tunnels; SCL method (bolted precast concrete segments)	Heathrow Central terminal	below (clearance 7m, skew angle: 69º)

Table 2: Parameters assumed for the J4 model for all the soil layers

Model parameters / Soil layers	C_1	C_2	C_3 (%)	α	γ	E_{dmin} (%)	E_{dmax} (%)	G_{min} (MPa)
London Clay B & A3	702	827	0.0001	1.1	0.62	0.005	0.3	2000
London Clay A2	767	903	0.0001	1.1	0.62	0.005	0.3	2000
Upper Lambeth Group	987	875	0.0001	1.1	0.850	0.003	0.3	2000
Lower Lambeth Group	1200	1100	0.0001	1.30	0.62	0.002	0.3	2000
	C_4	C_5	C_6 (%)	δ	λ	ε_{vmin} (%)	ε_{vmax} (%)	K_{min} (MPa)
London Clay B & A3	404	404	0.0035	1.8	0.34	0.001	0.2	2500
London Clay A2	404	404	0.0035	1.8	0.34	0.001	0.2	2500
Upper Lambeth Group	404	404	0.0035	1.8	0.34	0.001	0.2	2500
Lower Lambeth Group	265	850	0.0004	1.20	0.34	0.003	0.4	2500

Table 3: Parameters assumed for the Mohr-Coulomb model for all the soil layers

Model parameters / Soil layers	γ (kN/m^3)	c' (kPa)	ϕ'(°)	ν (°)	E' (MPa)	μ
Superficial deposits	18	0	25	12.5	10	0
London Clay B, A3 & A2	20	5	25	12.5	Small strain stiffness model used	
Upper Lambeth Group	20	10	28	14.0		
Lower Lambeth Group	20	0	36	18.0		

Figure captions.

Figure 1: Soil profile and general geometry adopted for the 3D analysis

Figure 2: Finite element mesh used for the 3D analysis

Figure 3: Initial a) permeability, b) pore water pressure and c) K_0 profiles adopted for the 3D analysis

Figure 4: Sequence of the step-by-step excavation adopted for the New Tunnel

Figure 5: Position of transverse monitoring sections relative to the existing line tunnel axis

Figure 6: (a) Transverse settlement troughs due to the New Tunnel excavation at the section directly above the Existing Tunnel axis and (b) Normalised surface troughs at the end of new excavation at different monitoring sections

Figure 7: Volume loss evolution due to the New Tunnel's excavation on different transverse sections

Figure 8: Longitudinal surface settlement profiles for monitoring line just above the New Tunnel axis for various New Tunnel face positions

Figure 9: Circumferential (a) hoop forces, (b) bending moments and (c) respective interaction diagram for Existing Tunnel's ring directly above the New Tunnel axis

Figure 10: Displaced shape and contours of absolute displacement of the existing line tunnel for different positions of the face of the New Tunnel excavation

Figure 11: Chords' span changes of different sections of the Existing Tunnel; field measurements vs FE analysis predictions

Figure 12: Longitudinal strains of the existing line tunnel along (a) crown or (b) invert predicted from FE analysis and (c) comparison with available field measurements

Figure 13: Comparison of circumferential a) , b) hoop forces and c, d) bending moments of the existing line tunnel lining for various positions of the New Tunnel excavation face for different face pressures of the EPBM

Figure 14: Comparison of different cross-sectional span changes for different face pressures of the EPBM for different Existing Tunnel cross sections

Figure 15: Longitudinal strain of existing line tunnel along the a) crown and the b) invert axis predicted from FE analysis with anisotropic stiffness shell elements used for the modelling of the existing line tunnel lining

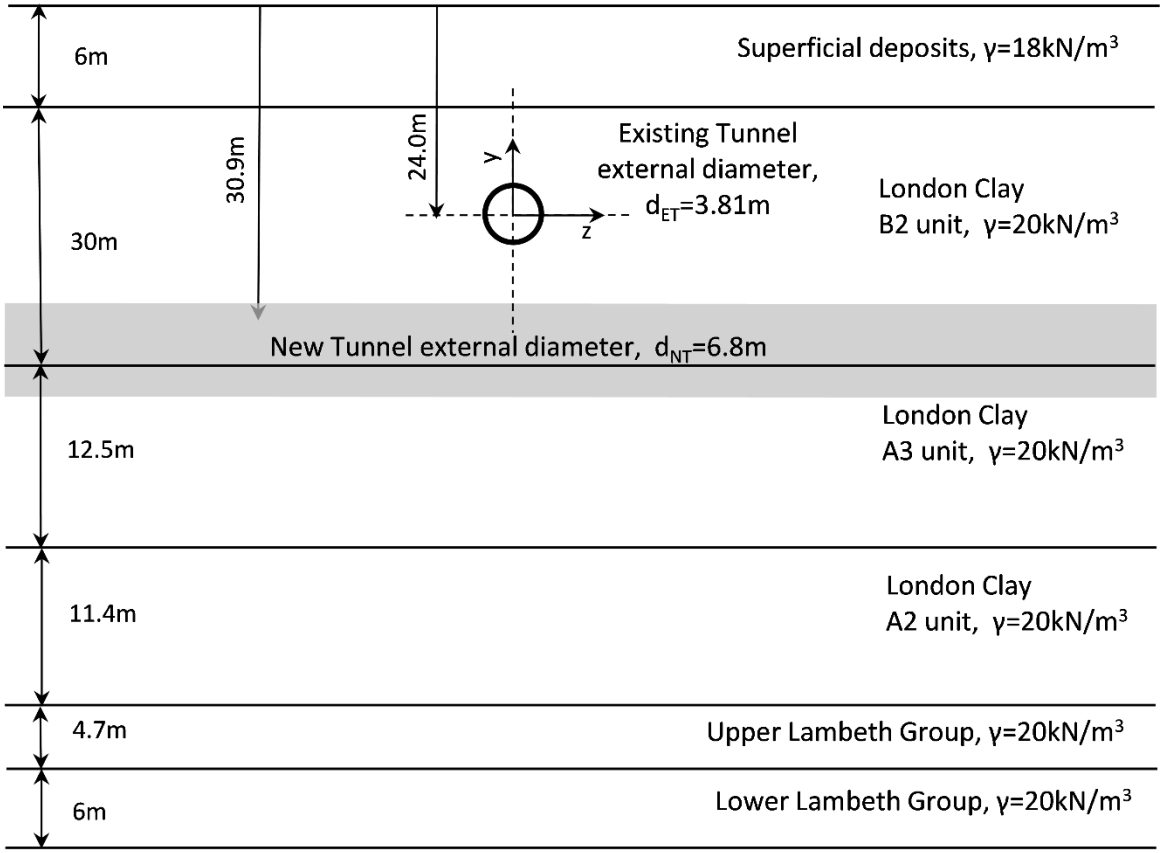

Figure 1: Soil profile and general geometry adopted for the 3D analysis

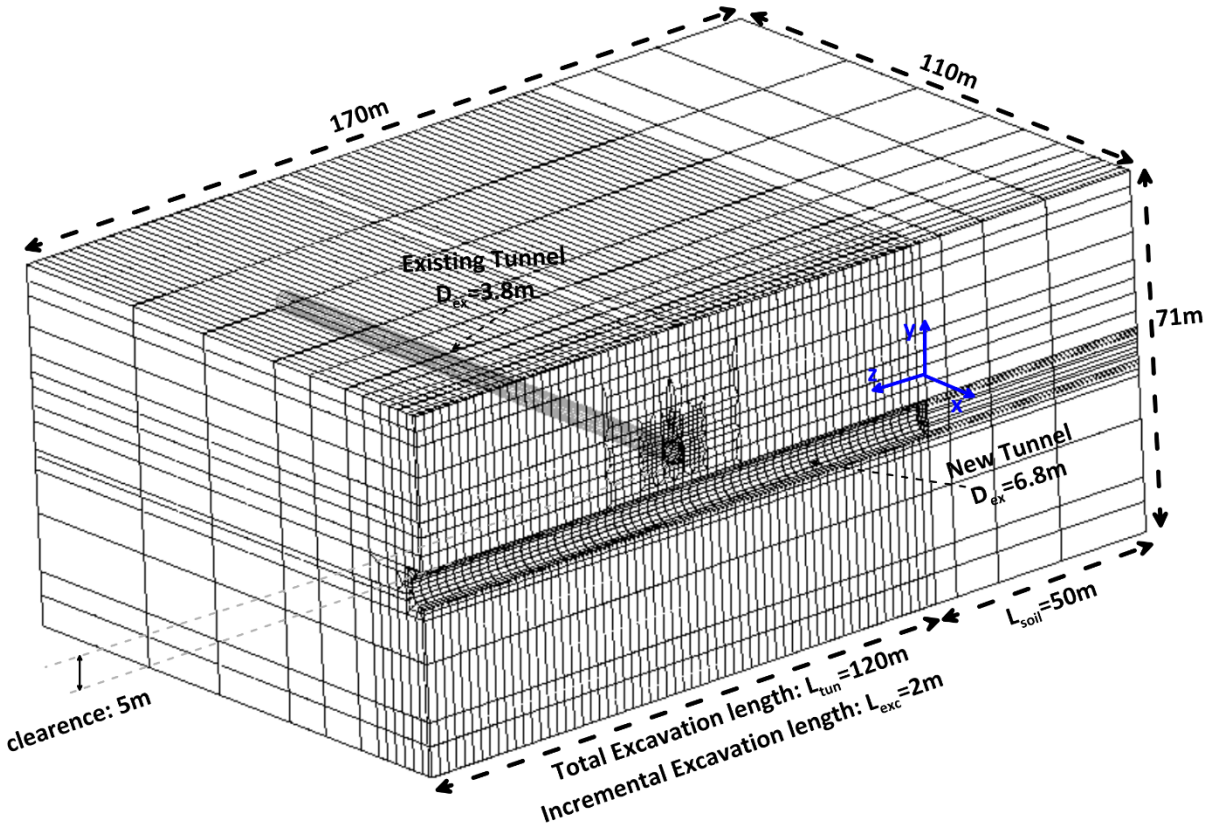

Figure 2: Finite element mesh used for the 3D analysis

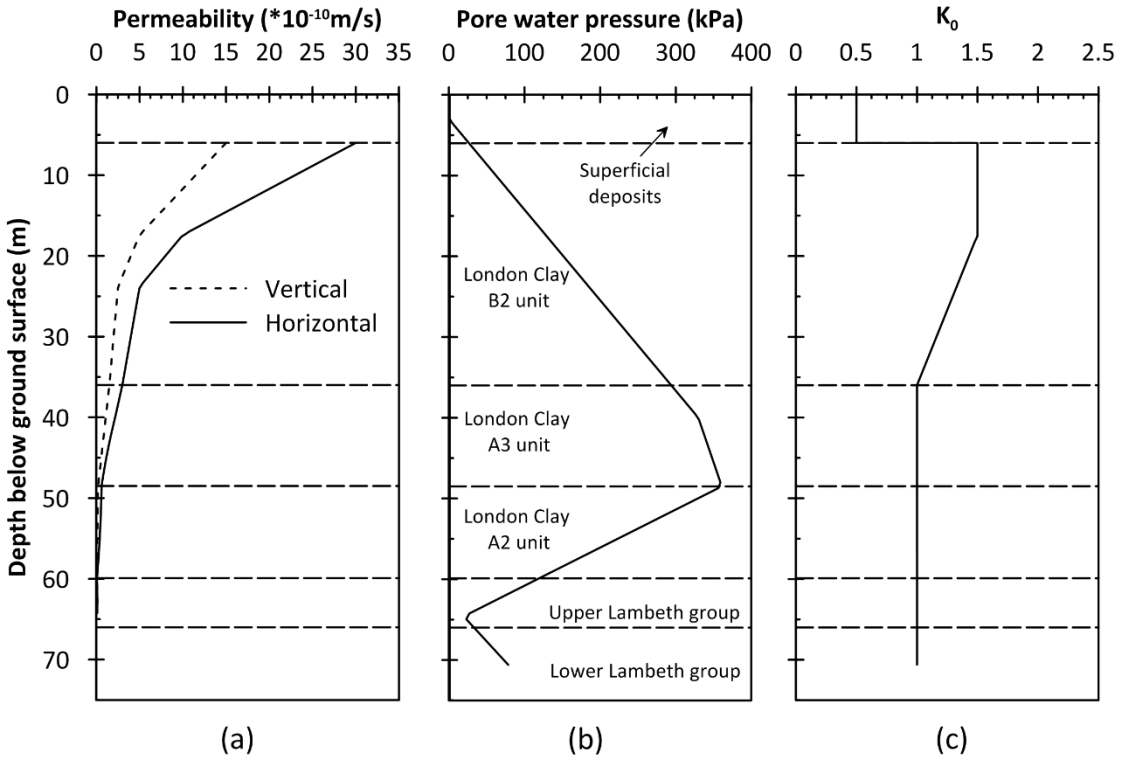

Figure 3: Initial a) permeability, b) pore water pressure and c) K_0 profiles adopted for the 3D analysis

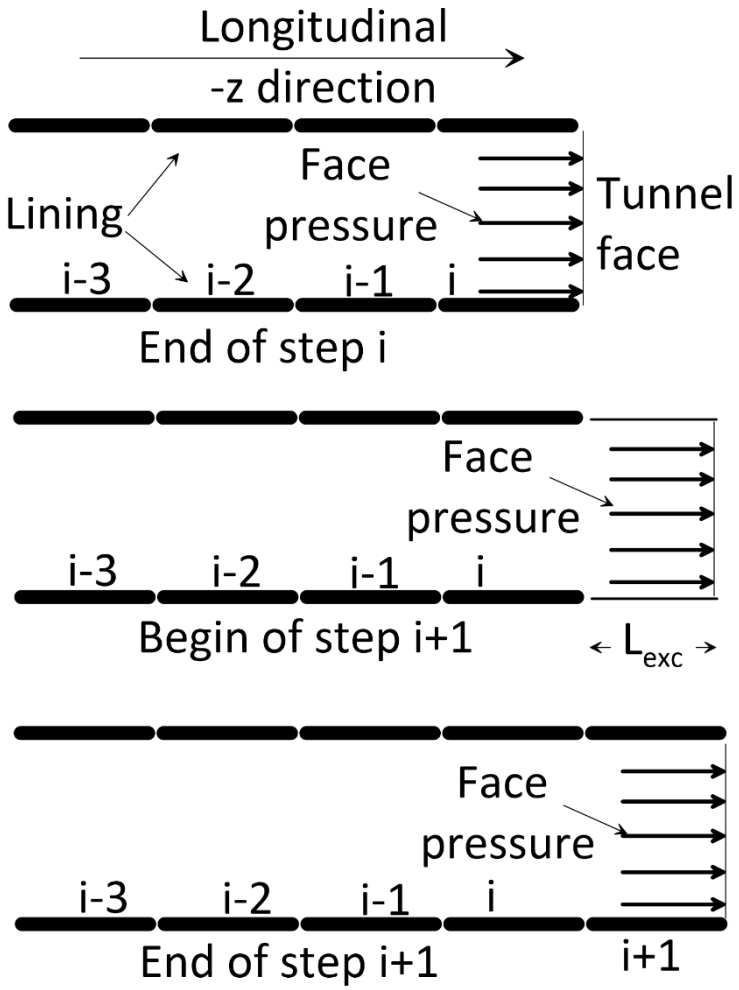

Figure 4: Sequence of the step-by-step excavation adopted for the New Tunnel

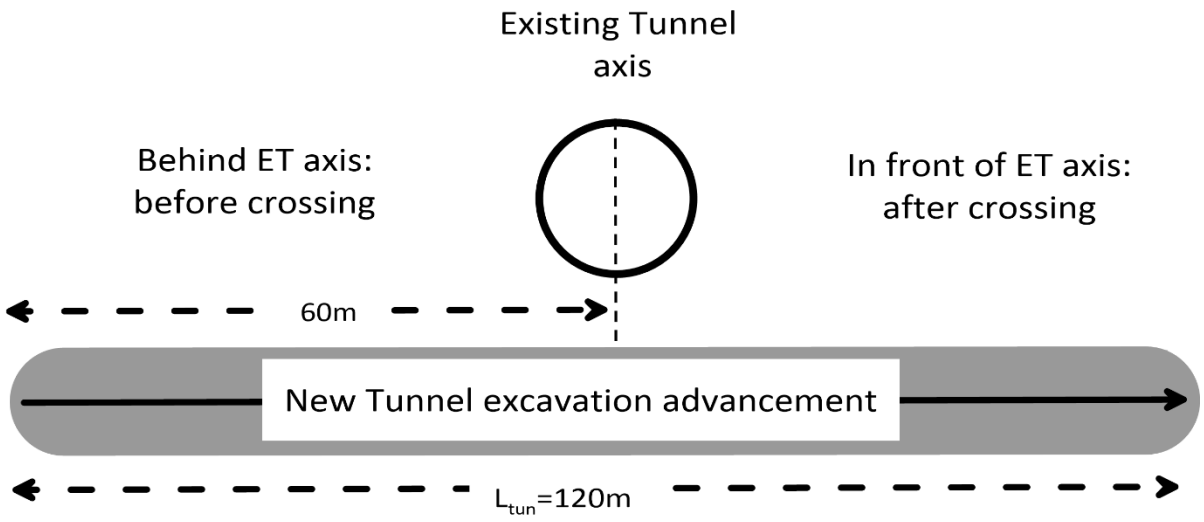

Figure 5: Position of transverse monitoring sections relative to the existing line tunnel axis

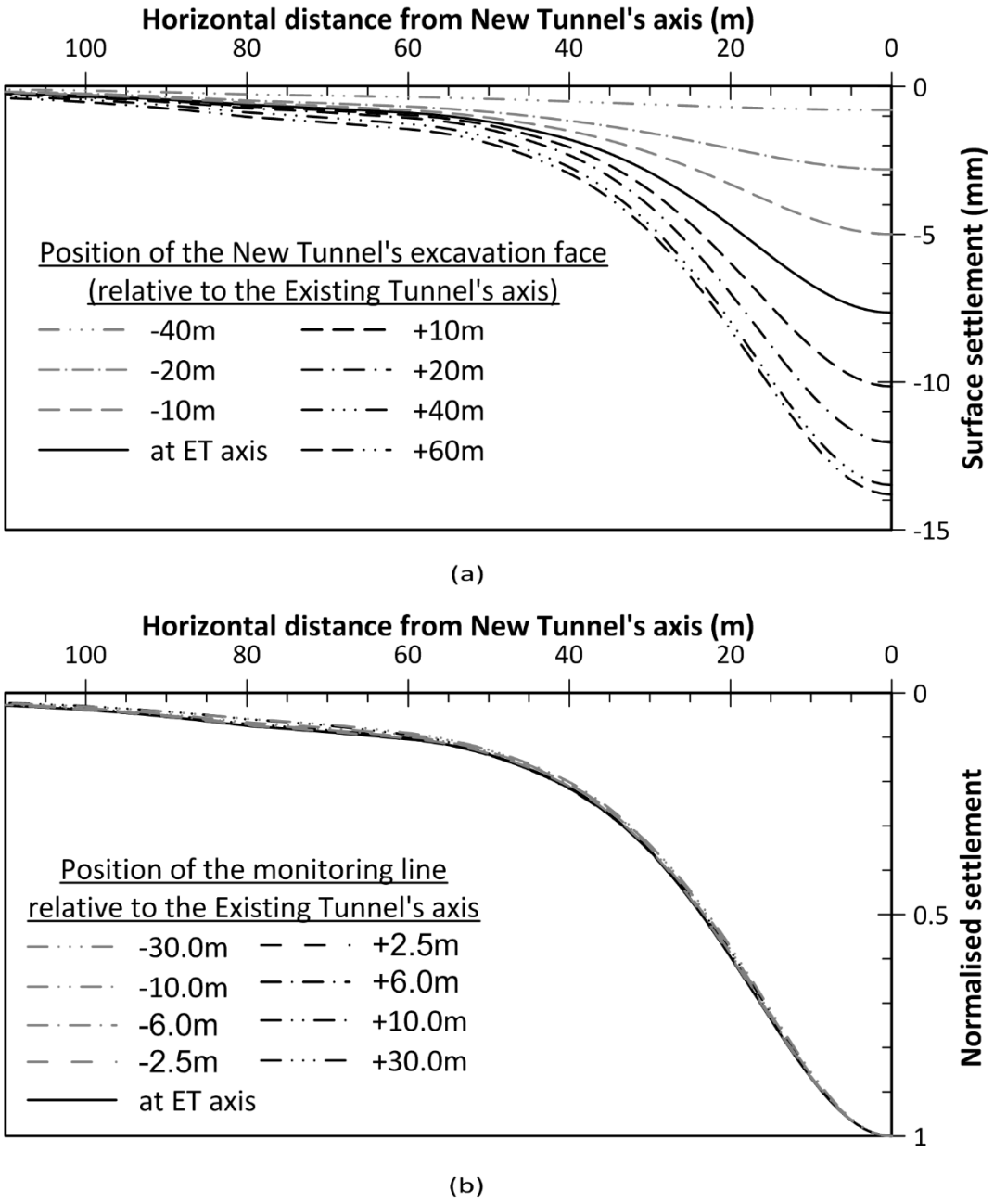

Figure 6: (a) Transverse settlement troughs due to the New Tunnel excavation at the section directly above the Existing Tunnel axis **and (b)** Normalised surface troughs at the end of new excavation at different monitoring sections

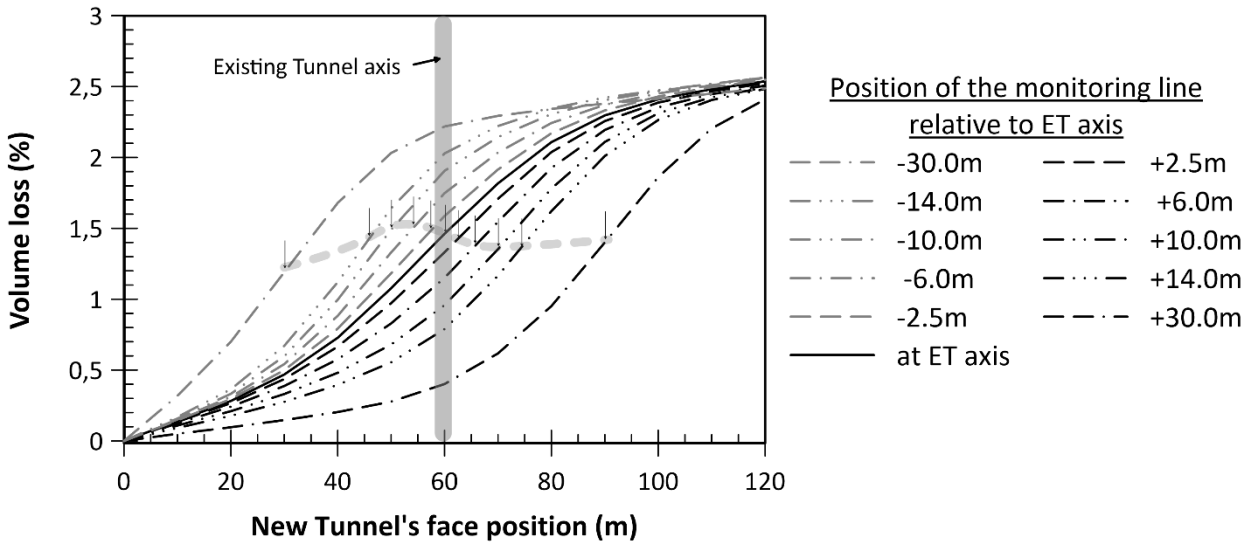

Figure 7: Volume loss evolution due to the New Tunnel's excavation on different transverse sections

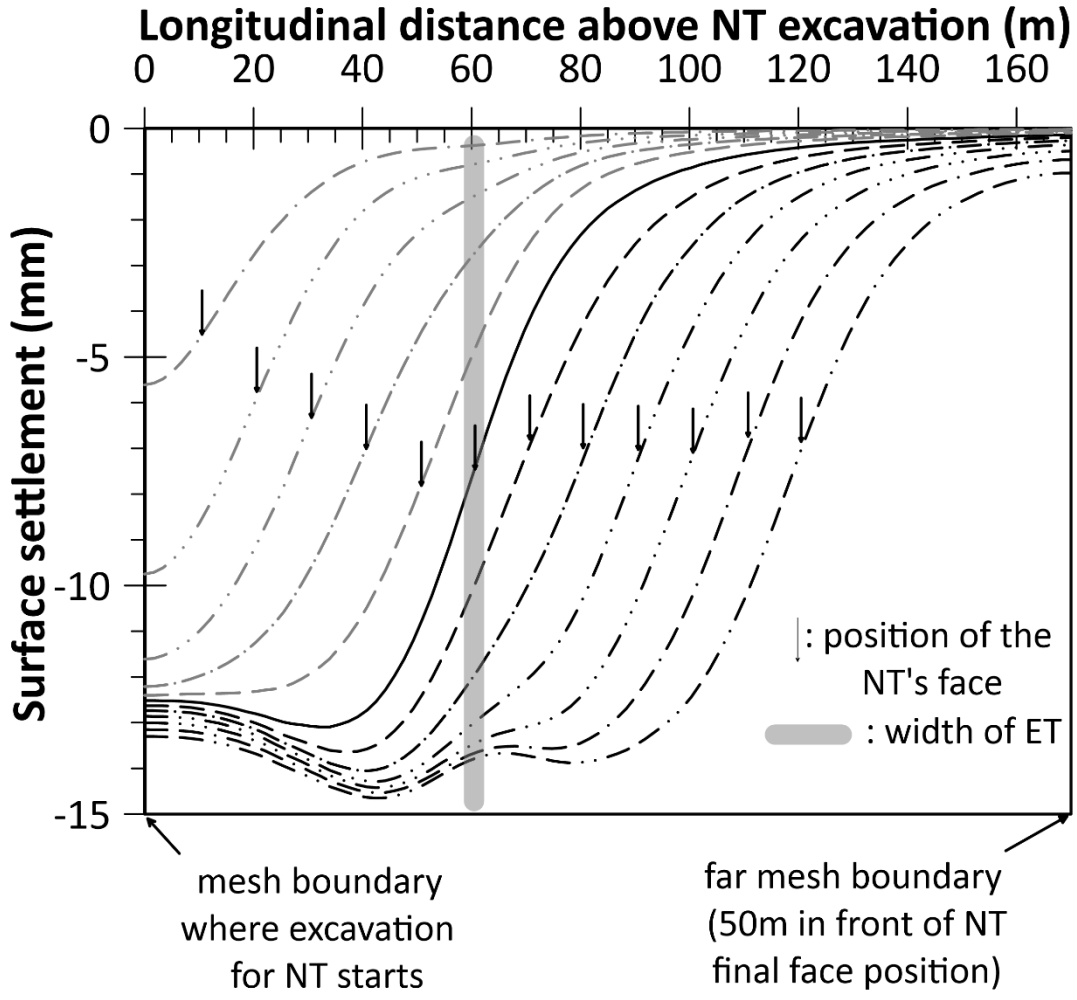

Figure 8: Longitudinal surface settlement profiles for monitoring line just above the New Tunnel axis for various New Tunnel face positions

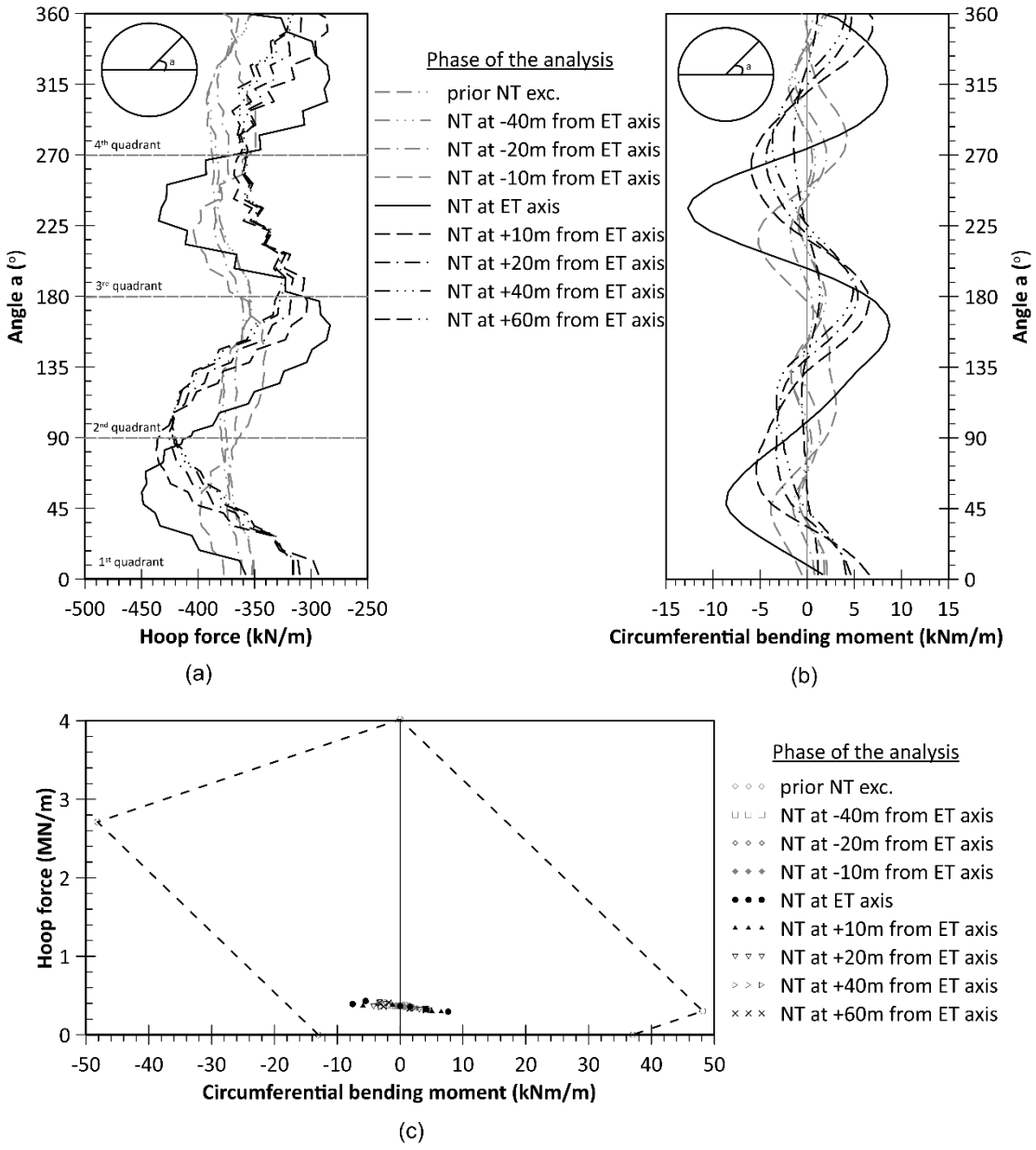

Figure 9: Circumferential (a) hoop forces, (b) bending moments and (c) respective interaction diagram for Existing Tunnel's ring directly above the New Tunnel axis

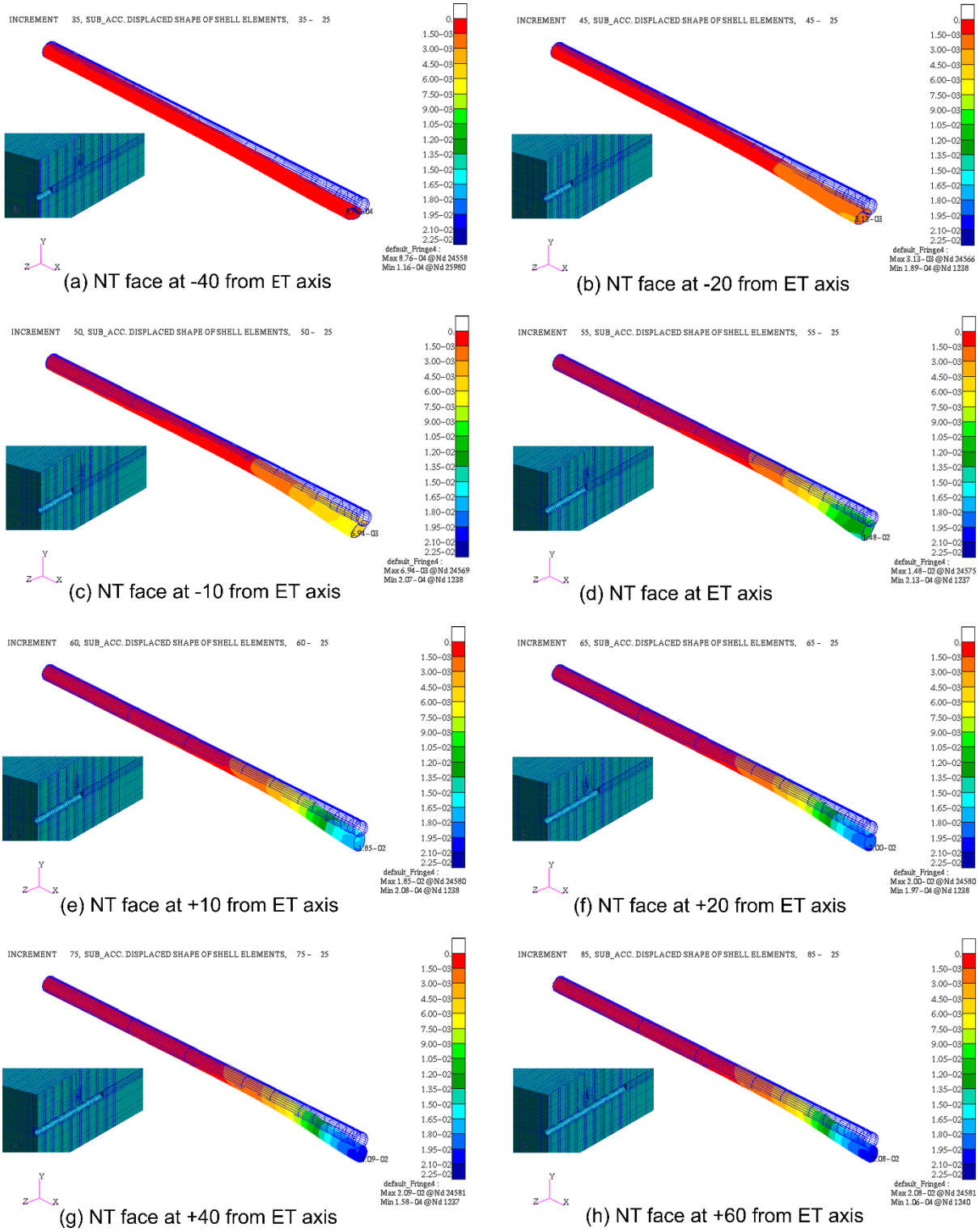

Figure 10: Displaced shape and contours of absolute displacement of the existing line tunnel for different positions of the face of the New Tunnel excavation

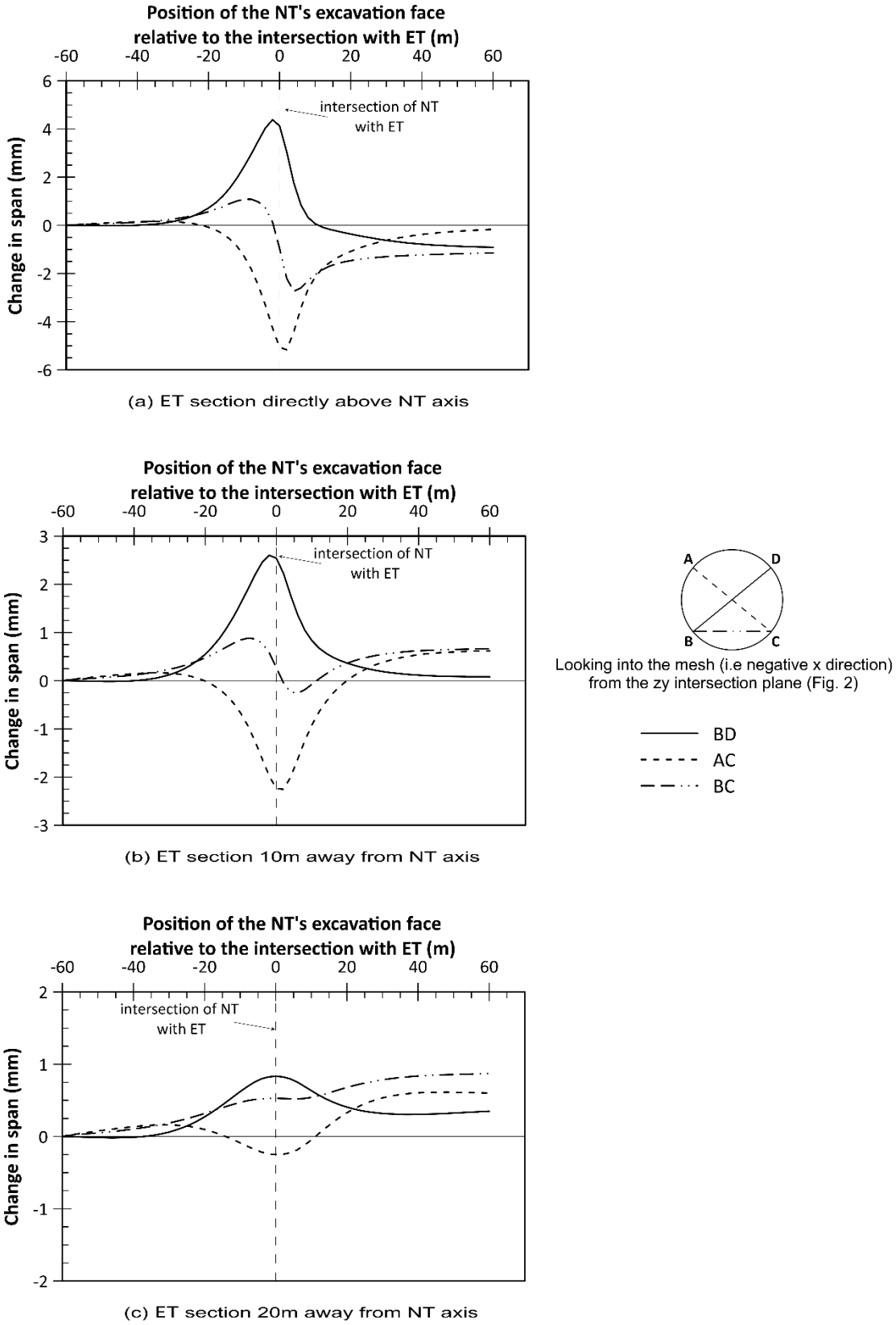

Figure 11: Chords' span changes of different sections of the Existing Tunnel; field measurements vs FE analysis predictions

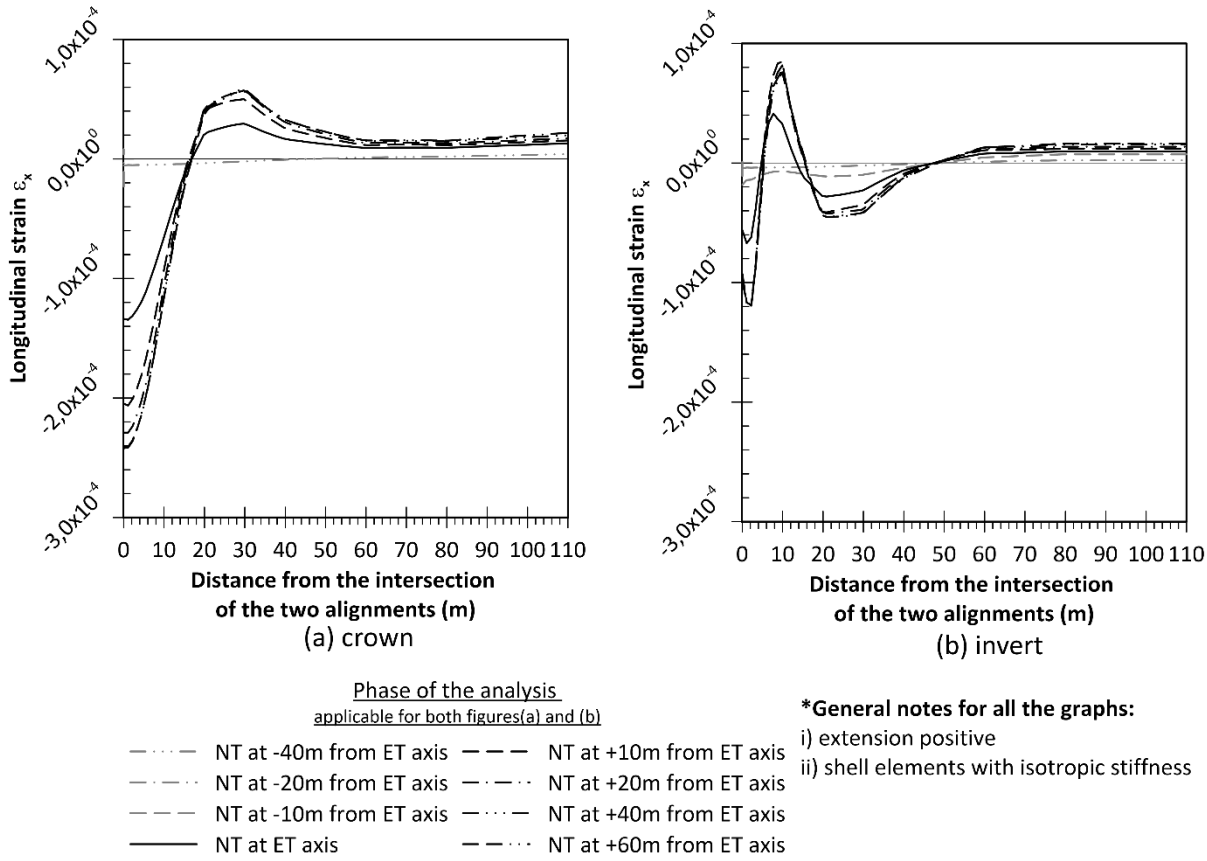

Figure 12: Longitudinal strains of the existing line tunnel along (a) crown or (b) invert predicted from FE analysis and (c) comparison with available field measurements

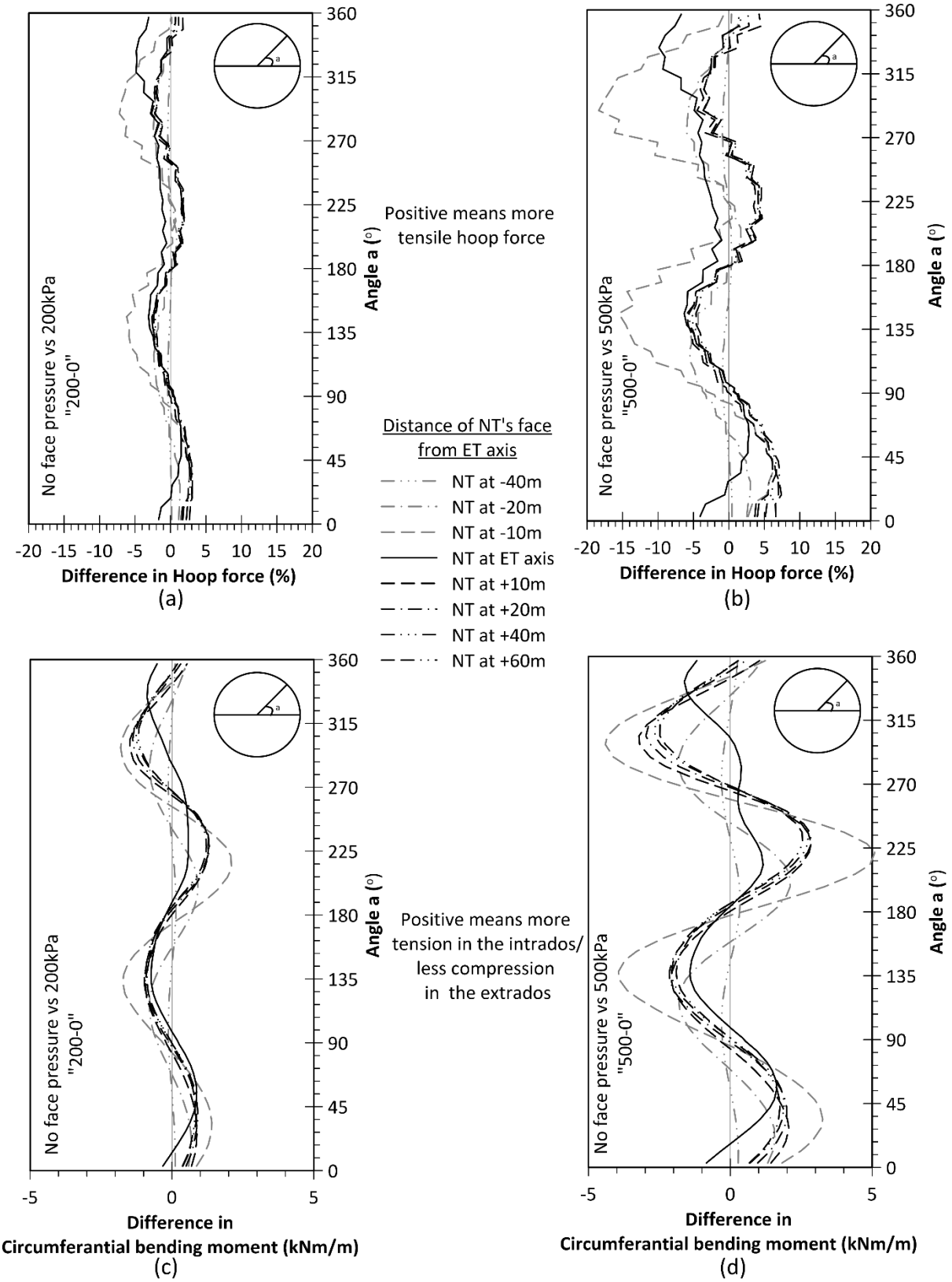

Figure 13: Comparison of circumferential a) , b) hoop forces and c, d) bending moments of the existing line tunnel lining for various positions of the New Tunnel excavation face for different face pressures of the EPBM

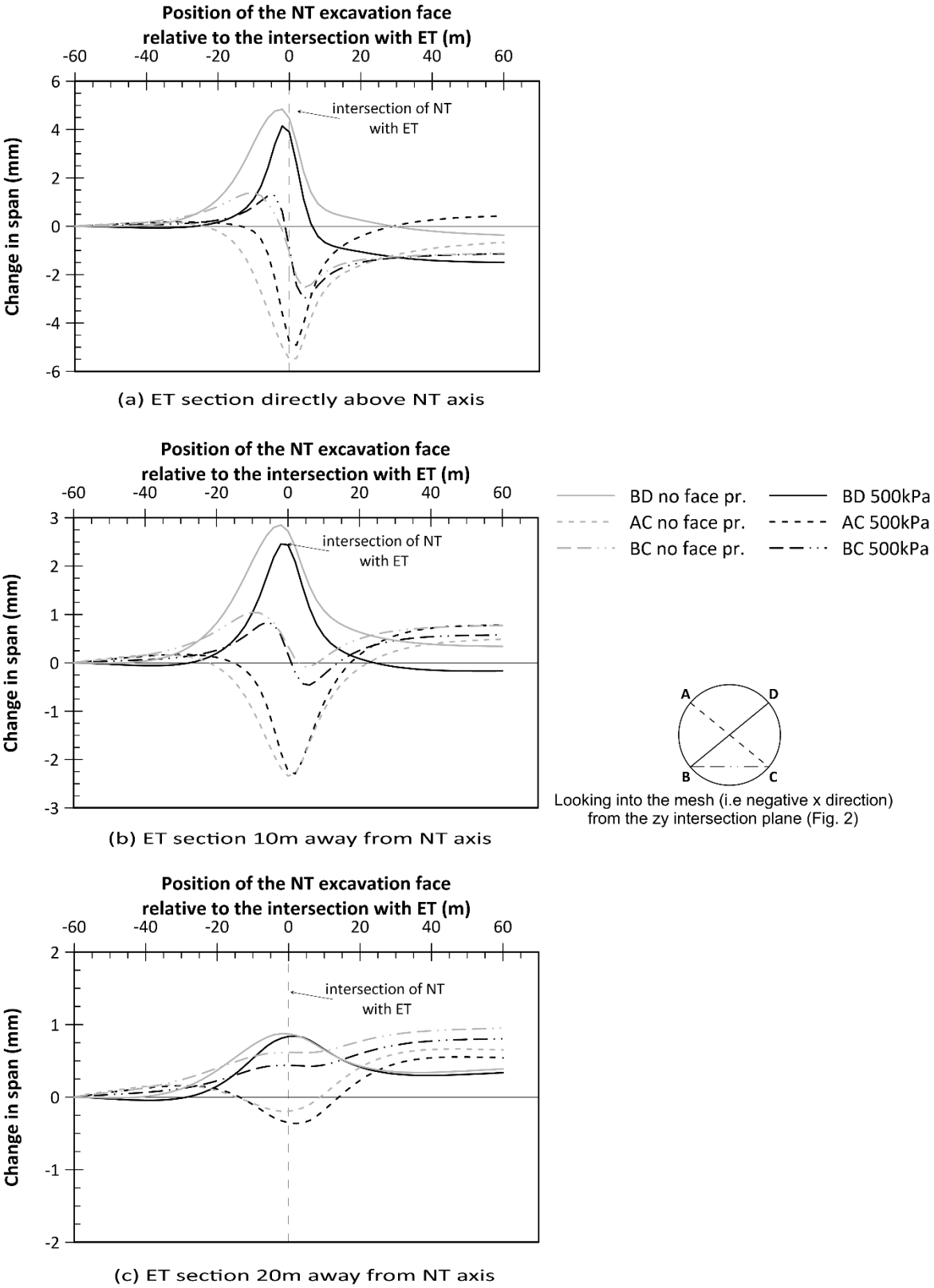

Figure 14: Comparison of different cross-sectional span changes for different face pressures of the EPBM for different Existing Tunnel cross sections

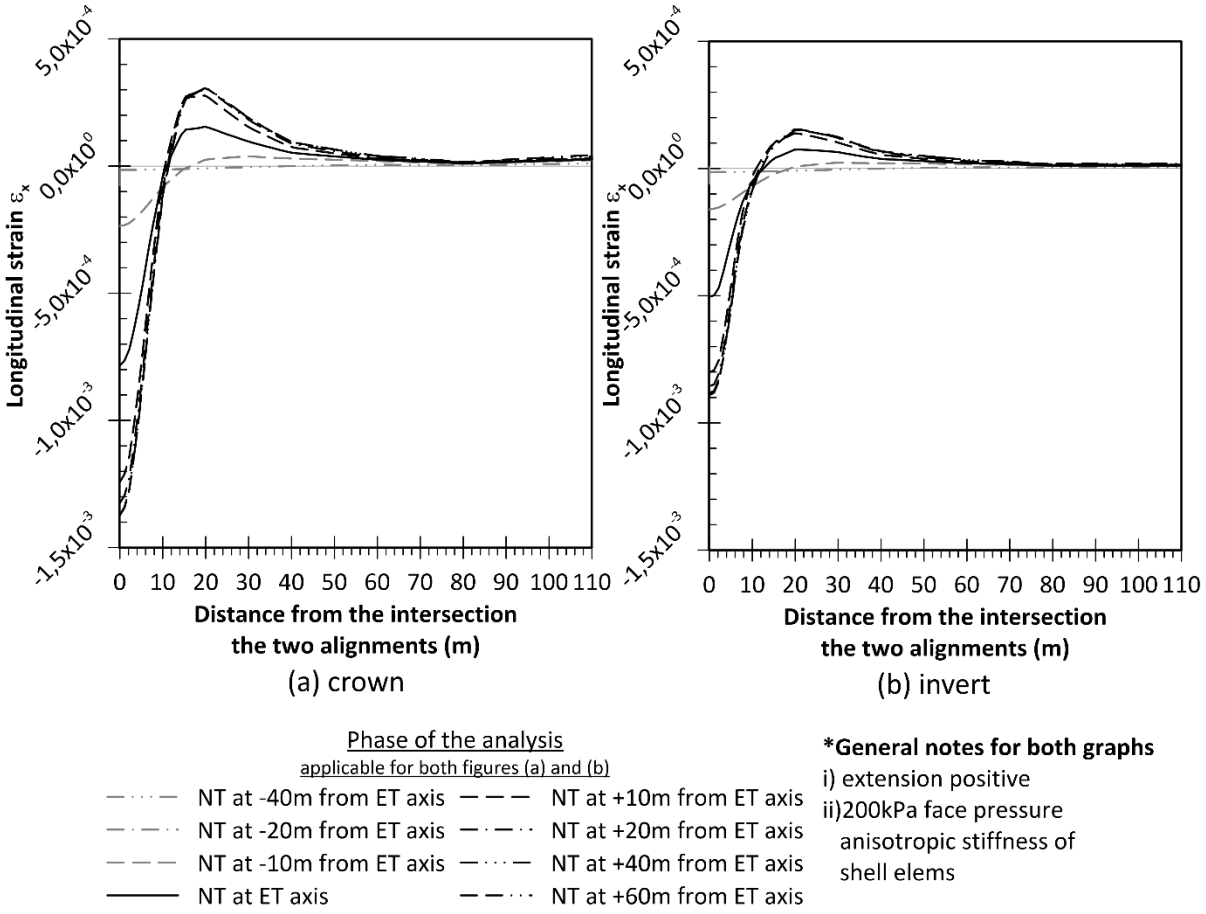

Figure 15: Longitudinal strain of existing line tunnel along the a) crown and the b) invert axis predicted from FE analysis with anisotropic stiffness shell elements used for the modelling of the existing line tunnel lining